HHS Public Access

Author manuscript

Neurochem Int. Author manuscript; available in PMC 2018 October 01.

Published in final edited form as:

Neurochem Int. 2017 October ; 109: 54–67. doi:10.1016/j.neuint.2017.03.020.

Updates to a ^{13}C metabolic flux analysis model for evaluating energy metabolism in cultured cerebellar granule neurons from neonatal rats

Mika B. Jekabsons[a], **Hoda M. Gebril**[b], **Yan-Hong Wang**[c], **Bharathi Avula**[d], and **Ikhlas A. Khan**[e]

[a]Department of Biology, 110 Shoemaker Hall, University of Mississippi, University, MS 38677, USA

[b]Feinberg School of Medicine, Northwestern University, Chicago, IL 60611, USA

[c]National Center for Natural Products Research, School of Pharmacy, University of Mississippi, University, MS 38677, USA

[d]National Center for Natural Products Research, School of Pharmacy, University of Mississippi, University, MS 38677, USA

[e]Department of Biomedical Sciences and National Center for Natural Products Research, School of Pharmacy, University of Mississippi, University, MS 38677, USA

Abstract

A hexose phosphate recycling model previously developed to infer fluxes through the major glucose consuming pathways in cultured cerebellar granule neurons (CGNs) from neonatal rats metabolizing [1,2-$^{13}C_2$]glucose was revised by considering reverse flux through the non-oxidative pentose phosphate pathway (PPP) and symmetrical succinate oxidation within the tricarboxylic acid (TCA) cycle. The model adjusts three flux ratios to effect ^{13}C distribution in the hexose, pentose, and triose phosphate pools, and in TCA cycle malate to minimize the error between predicted and measured ^{13}C labeling in exported lactate (i.e., unlabeled, single-, double-, and triple-labeled; M, M1, M2, and M3, respectively). Inclusion of reverse non-oxidative PPP flux substantially increased the number of calculations but ultimately had relatively minor effects on the labeling of glycolytic metabolites. From the error-minimized solution in which the predicted M-M3 lactate differed by 0.49% from that measured by liquid chromatography-triple quadrupole mass spectrometry, the neurons exhibited negligible forward non-oxidative PPP flux. Thus, no glucose was used by the pentose cycle despite explicit consideration of hexose phosphate

Correspondence to: Mika B. Jekabsons.

Author contribution statement

HMG, BA, YHW, and IAK contributed to experimental design and performed experiments; MBJ developed the model and approach. MBJ and YHW wrote the paper.

Declarations of Interest

The authors declare no conflicts of interest.

recycling. Mitochondria consumed only 16% of glucose while 45% was exported as lactate by aerobic glycolysis. The remaining 39% of glucose was shunted to pentose phosphates presumably for *de novo* nucleotide synthesis, but the proportion metabolized through the oxidative PPP vs. the reverse non-oxidative PPP could not be determined. The lactate exported as M1 (2.5%) and M3 (1.2%) was attributed to malic enzyme, which was responsible for 7.8% of pyruvate production (vs. 92.2% by glycolysis). The updated model is more broadly applicable to different cell types by considering bi-directional flux through the non-oxidative PPP. Its application to cultured neurons utilizing glucose as the sole exogenous substrate has demonstrated substantial oxygen-independent glucose utilization by aerobic glycolysis as well as the oxidative PPP and/or reverse non-oxidative PPP, but negligible glucose consumption by the pentose cycle.

Keywords

mitochondria; pentose phosphate pathway; glycolysis; bioenergetics; malic enzyme

1. Introduction

The brain's utilization of glucose exceeds that predicted from the rate of oxygen consumption (Boyle et al., 1994; Dienel and Cruz, 2016; Madsen et al., 1995; Vaishnavi et al., 2010). Such mitochondrial-independent glucose consumption varies regionally, developmentally, and according to neuronal activity (Goyal et al., 2014; Madsen et al., 1995; Settergren et al., 1976; Vaishnavi et al., 2010), and reflects 'aerobic glycolysis' and pentose phosphate pathway (PPP) activities. Aerobic glycolysis involves glucose conversion to lactate despite adequate oxygen availability for its oxidation by mitochondria. Glucose consumption by the oxidative PPP or by the combined oxidative/non-oxidative pentose cycle involves its respective conversion to CO_2 and pentose phosphates, or CO2 and glyceraldehyde-3-phosphate. Glial cells may account for a considerable proportion of oxygen-independent glucose consumption in the adult brain given their high aerobic glycolytic profile and PPP activity (Amaral et al., 2011; Amaral et al., 2016; Belanger et al., 2011); however, the contribution by neurons can be significant and may profoundly influence brain development and plasticity, as well as susceptibility to neurodegeneration. Regions of higher non-mitochondrial glucose consumption correlate with greater expression of markers for synapse formation, plasticity, and remodeling (Goyal et al., 2014), although it is unknown to what extent provision of pentose phosphates, NADPH, or lactate support these communicative processes. Additionally, neuronal vulnerability to stress can be affected by oxidative PPP capacity to supply NADPH for removal of reactive oxygen species and protection of protein thiols (Herrero-Mendez et al., 2009). Assessment of glucose used by the oxidative PPP (for supplying NADPH and pentose phosphates, the latter of which is used for nucleotide synthesis) and by the pentose cycle (for supplying NADPH and 'excess' pentose phosphates not used for nucleotide synthesis) is challenging because of carbon recycling that occurs from the pentose cycle to the oxidative PPP. For glucose passing through the pentose cycle, two-thirds returns to glycolysis as fructose-6-phosphate/glucose-6-phosphate and is subject to recycling, while the remaining one-third is consumed by conversion to CO_2 and glyceraldehyde-3-phosphate. The goal of this study was to

develop an approach to determine the proportion of glucose used by cultured neurons for the oxidative PPP, the pentose cycle, anaerobic glycolysis, and mitochondrial respiration.

Pathway fluxes can be inferred from the rates of exogenous substrate consumption, the rates of metabolic waste production, and the distribution of isotope within one or more metabolites from catabolism of an isotopically labeled substrate. Mathematical models designed to reproduce the isotope enrichment pattern in one or more metabolites can be developed to infer unknown fluxes from the measured rates and a set of constraints that effectively define the system. These constraints include (a) the number, connectedness, and compartmentation of the reactions (i.e., the system structure), (b) the carbon atom rearrangements for each substrate/product pair, (c) the stoichiometries of the reactions, and (d) any assumptions about pathway behavior (e.g., reversibility). We recently developed a model for quantifying fluxes through the major glucose consuming reaction blocks in primary cerebellar granule neurons metabolizing [1,2-$^{13}C_2$]glucose (Gebril et al., 2016). The model quantitatively tracks ^{13}C distribution in glucose-6-phosphate/fructose-6-phosphate (hexose phosphates-HxP) from the recycling of glucose carbons via the non-oxidative PPP back to the oxidative PPP, and ^{13}C distribution in malate by carbon rearrangements within the tricarboxylic acid (TCA) cycle. The latter distribution was considered since ^{13}C in pyruvate entering the TCA cycle can be recycled back to pyruvate via cytoplasmic and mitochondrial malic enzyme. The quantitative analysis is based on measurements of glucose consumption, lactate production, and mitochondrial respiration, and theoretical predictions on the extent of HxP recycling within the PPP (Gebril et al., 2016; WOOD and KATZ, 1958). The measured ^{13}C distribution in exported lactate (i.e., the fraction having zero, one, two, or three ^{13}C atoms- denoted as M, M1, M2, and M3, respectively) is reproduced from calculations (predictions) of ^{13}C distributions in HxP, malate, triose phosphates (TrP; glyceraldehyde-3-phosphate and dihydroxyacetone phosphate), and pyruvate, which in turn are determined from optimizing the relative contributions of the non-oxidative PPP, glycolysis, the TCA cycle, and malic enzyme to producing these metabolites. One notable assumption made about pathway behavior was unidirectional flux through the non-oxidative PPP (Gebril et al., 2016), despite the known reversible nature of this pathway; this served to minimize the number of calculations required for assessing ^{13}C distribution in HxP and TrP. This article describes revisions to the original model that improve its accuracy and applicability to different cell types by accounting for ^{13}C randomization in HxP, pentose phosphates, and TrP resulting from reverse non-oxidative PPP flux, and in malate by symmetrical metabolism of succinate in the TCA cycle. The updates prompted re-analysis of ^{13}C distribution in lactate from cerebellar granule neurons metabolizing [1,2-$^{13}C_2$]glucose previously reported in (Gebril et al., 2016). The revised model and measurements indicate negligible non-oxidative PPP flux, contrary to our original conclusion of extensive pentose cycle activity.

2. Materials and Methods

Preparation of rat cerebellar granule neuron cultures, flux measurements (rates of glucose consumption, lactate production, and mitochondrial respiration), lactate labeling from [1,2-$^{13}C_2$]glucose, and lactate derivatization with 3-nitrophenylhydrazine were detailed in (Gebril et al., 2016). Unlabeled and [3-^{13}C]lactate (Cambridge Isotope Laboratories,

Andover, MA, USA) standards, separately and mixed at 7.6:1 M:M1 ratio, were processed with the unknowns. The derivatized samples were diluted 100-fold in 80% methanol and analyzed on a Waters ACQUITY I-Class UPLC™ system coupled with a Waters Xevo TQ-S triple quadrupole mass spectrometer (Waters Corp, Milford, MA, USA). The separation (1 μL) was carried out on a Waters Acquity UPLC™ BEH C18 column (50mm × 2.1mm i.d., 1.7 μm). Sample and column temperatures were maintained at 10 °C and 40 °C, respectively. The mobile phase consisted of water containing 0.1% formic acid (v/v) (A) and acetonitrile with 0.1% formic acid (B). The analysis was performed using the following gradient elution at a flow rate of 0.50 mL/min: 0–2.5 min, 5% B to 18% B; 2.5–3 min, 18% B to 100% B. Each run was followed by a 2.5 min wash with 100% B and an equilibration period of 2.5 min with the initial conditions. The strong and weak solutions used to wash the auto sampler were methanol/acetonitrile/isopropanol/water (25:25:25:25, v/v/v/v/v) and methanol/water (70:30, v/v), respectively. The effluent was introduced into the TQ-S mass spectrometer equipped with electrospray ionization in negative ion mode (ESI-) for quantification of the analytes. Detection was obtained by Multiple Reaction Monitoring (MRM) mode including two MRMs for confirmation of the analytes. The quantification of analytes 224, 225, 226, and 227 (the expected masses for M, M1, M2, and M3 lactate derivatized with 3-nitrophenylhydrazine, respectively; all had 1.84 min retention times) was acquired with transitions of deprotonated ion at m/z 224.04 → 152.06 for M, 225.04 → 152.06 for M1, 226.04 → 152.06 for M2, and 227.04 → 152.06 for M3. The dwell Rme was 20 msec at cone voltage=44 V and collision energy=14 eV for each transition. The ESI–MS/MS parameters were set as follows: capillary voltage, 1.20 kV; cone voltage, 44 V; source temperature, 150 °C; desolvation temperature, 600 °C; desolvation gas flow, 600 L/h, cone gas flow, 200 L/h. Nitrogen was used as desolvation and cone gas. Argon (99.99% purity) was introduced as the collision gas into the collision cell at a flow rate of 0.15 mL/min. Data acquisition was carried out with MassLynx 4.1 software (Waters Corp., Milford, MA, USA). Monte Carlo simulations were performed using the means and standard errors of M-M3 lactate (Table 3) as previously described (Gebril et al., 2016) except that three of four labels were simulated and the fourth calculated so that M+M1+M2+M3=1.

3. Results and Discussion

3.1. Inferring fluxes from ^{13}C distribution in lactate

3.1.1 Metabolic structure and measured fluxes—A major goal was to develop a model that accounts for ‘recycling’ processes which affect ^{13}C distribution in exported lactate so that fluxes through the major glucose consuming pathways can be determined from a relatively small number of measurements. Oxidative and non-oxidative PPP activities were a particular focus because of extensive carbon reshuffling from the pentose cycle and associated HxP recycling, and reverse flux through the non-oxidative PPP. Overlooking such processes would introduce errors to the fluxes inferred from isotope enrichment of glycolytic metabolites such as lactate when these fluxes are significant. Furthermore, carbon rearrangement within the TCA cycle is extensive and can affect ^{13}C deposition in lactate through reactions such as malic enzyme that recycle carbon to pyruvate. Malic enzyme has both cytoplasmic and mitochondrial isoforms, the latter of which dominates in neurons (McKenna et al., 2000; Zwingmann and Leibfritz, 2007). Pyruvate recycling may thus occur

primarily in the matrix, after which transport by the pyruvate carrier would allow equilibration with the cytoplasmic pyruvate pool. Regardless of the pathway taken by malate (malate export then oxidation in the cytoplasm, or malate oxidation in the matrix followed by pyruvate export), the effect on label distribution in the cytoplasmic pyruvate pool is equivalent. The model assumed that pyruvate derived from malic enzyme mixed uniformly with that derived from glycolysis; additionally, the pyruvate derived from glucose metabolized by the pentose cycle and then glycolysis was assumed to enter the same pool, so that the ^{13}C pattern in extruded lactate reflected the contribution of each pathway to labeling this pool. This assumption may not be valid, as others have concluded that pyruvate derived from the pentose cycle, glycolysis, and/or the TCA cycle may form distinct pools that are preferentially imported by mitochondria or exported as lactate, respectively (Brekke et al., 2012; McKenna et al., 2012). To evaluate the contribution of the pentose cycle, glycolysis, and malic enzyme to ^{13}C enrichment in exported lactate, probability calculations were developed in Excel to quantitatively track ^{13}C reshuffling in the PPP and the tricarboxylic acid cycle of cultured neurons metabolizing [1,2-$^{13}C_2$]glucose as the only exogenous substrate (Gebril et al., 2016). The objective was to find the relative activities (i.e., their respective contributions to producing a metabolite) of the PPP and malic enzyme that yielded a predicted ^{13}C distribution in lactate which reflected that measured by LC-MS/MS. Based on previous work with hepatocytes (Ainscow and Brand, 1999), twelve interconnected reaction ‘blocks’ were considered as core components of the major glucose consuming pathways (Fig. 1). Their structure is such that all fluxes could be inferred from the LC-MS/MS data provided that (a) the rates of glucose consumption, lactate production, and mitochondrial respiration were determined, (b) the system maintained an isotopic and metabolic steady-state, and (c) the reaction stoichiometries were known. This article describes revisions to the original probability calculations to account for ^{13}C reshuffling by two processes overlooked in the original model: reverse flux through the non-oxidative PPP (Fig. 1; J_{3f} and J_{3r} denote the forward and reverse fluxes, respectively) and symmetrical succinate oxidation in the TCA cycle.

3.1.2. Qualitative tracking of carbon rearrangements in the non-oxidative PPP

—When NADPH demand by reactions involved in redox homeostasis and lipid biosynthesis exceeds the demand for ribulose-5-phosphate (Ri5P) by reactions involved in *de novo* nucleotide synthesis, then the oxidative PPP will overproduce Ri5P. For this condition, regulation of Ri5P is achieved by conversion of the excess to the glycolytic intermediates fructose-6-phosphate (F6P) and glyceraldehyde-3-phosphate (G3P) through ‘forward’ non-oxidative PPP flux. Two-thirds of the original G6P carbons deposited as excess pentose phosphates return as the hexose equivalent F6P (J_{3af}; and one-third enters glycolysis as TrP, J_{3bf}), and can either be used for glycolysis or recycled into the oxidative PPP upon conversion to G6P by hexose phosphate isomerase. Glucose utilization by the combined pentose cycle involves its conversion to CO_2 in J_1 and to TrP in J_{3f} (equivalent to $J_{3f}/6 + J_{3bf}/2$ vs. non-cyclic utilization by the oxidative PPP and reactions synthesizing nucleotides, equivalent to $(J_1 - J_{3f})/6 + 5 * J_9/6$). For accurate flux analysis with [1,2-$^{13}C_2$]glucose, it is important to consider the reshuffling of G6P carbons not only as they return through the non-oxidative PPP, but also as they recycle one or more times through the oxidative PPP.

The first step in tracking ^{13}C reshuffling by the 'forward' PPP is to delineate the carbon transfers within the individual reactions. This is straightforward in the oxidative PPP, where the carbon order in G6P is retained until 6-phosphogluconate dehydrogenase, which catalyzes removal of carbon 1 as $^{13}CO_2$ to yield [1-^{13}C]Ri5P as substrate for the non-oxidative PPP. The first two parallel reactions of the 'forward' non-oxidative PPP are isomerizations of Ri5P by phosphopentose isomerase and phosphopentose epimerase that do not affect the order of carbons. The isomerase converts the carbon 2 ketose to a carbon 1 aldose, yielding ribose-5-phosphate (R5P); the epimerase reverses the stereochemistry of the carbon 3 hydroxyl in Ri5P to yield the ketose xylulose-5-phosphate (X5P). Transketolase has broad substrate specificity and catalyzes the transfer of two carbons from a ketose (having specific hydroxyl configurations surrounding the keto group) to carbon 1 of an aldose (Kochetov and Solovjeva, 2014). In this case, the first two carbons of X5P are transferred to carbon 1 of R5P, forming the new ketose sedoheptulose-7-phosphate (S7P) and the three carbon aldose G3P (Fig. 2). These 'forward' products also satisfy the substrate requirements for transketolase, so the reverse reaction in which the first two carbons of S7P are transferred to carbon 1 of G3P also occurs. In developing the model, G3P formed by the first forward transketolase reaction was assumed a transient, PPP-specific metabolite that does not equilibrate with the glycolytic TrP pool.

Transaldolase catalyzes transfer of the first 3 carbons of S7P to carbon 1 of the aldose acceptor G3P, generating the new ketose/aldose pair F6P and erythrose-4-phosphate (E4P), both of which are adequate substrates for the reverse transaldolase reaction (Samland and Sprenger, 2009). Carbons 4–6 in F6P (F6P1 in Fig. 2) retain their original positions from G6P converted to X5P (G6P2 in Fig. 2), while carbons 2 and 3 now reside at positions 1 and 2; position 3 is occupied by carbon 2 derived from G6P converted to R5P (G6P1 in Fig. 2). The final forward reaction is a second transketolase two carbon ketose transfer from a second X5P (from G6P3 in Fig. 2) to the E4P aldose, yielding F6P2 and one G3P, the latter of which equilibrates with the glycolytic TrP pool. Positions 1 and 2 of the second F6P are from carbons 2 and 3 of G6P3, while the remaining positions 3–6 are preserved from G6P1. The TrP carbons derive from positions 4–6 of G6P3. From the forward reaction, only carbon positions 2 and 3 in the initial G6P substrates are rearranged in F6P. With [1,2-$^{13}C_2$]glucose, the TrP produced from this pentose cycle lack ^{13}C since they are derived from positions 4–6, which are not reshuffled. One of three fates was considered for F6P formed by the non-oxidative PPP: (a) it can equilibrate with G6P and recycle into the oxidative and non-oxidative PPP for additional carbon reshuffling, (b) it can equilibrate with G6P and then be processed by glycolysis to TrP, or (c) it can equilibrate with G6P, followed by partial glycolytic processing to F6P or TrP, and then return to the pentose pool through reverse flux of the non-oxidative PPP. Note that the model assumed rapid equilibration of F6P with G6P such that they form a single pool with identical ^{13}C distributions.

3.1.3. Quantitative HxP recycling with a reversible non-oxidative PPP—Isotope distribution in the HxP pool was calculated from the contribution of J_0 (glucose uptake/phosphorylation) and J_{3af} (forward non-oxidative PPP flux, expressed as HxP formed per unit time) to HxP production (Fig. 1), together with the relative yield of each label produced

by the respective blocks. Since the carbons in glucose are not reordered by J_0, the contribution of J_0, to labeling the HxP pool (as [1,2- $^{13}C_2$]G6P/F6P) is

$$1 - \frac{J_{3af}}{J_0 + J_{3af}} \quad (1)$$

Note that the rate of exogenous [1,2-$^{13}C_2$]glucose entering the HxP pool also reflects the fraction of the total pool not returning due to carbon loss as CO_2/TrP in the pentose cycle, as R5P incorporated into nucleotides, and as pyruvate formed from glycolysis. The fraction of HxP which leaves the pool and returns (as one of eight possible labels from ^{13}C reshuffling one or more times in the non-oxidative PPP) (Gebril et al., 2016) is

$$\frac{J_{3af}}{J_0 + J_{3af}} \quad (2)$$

It follows that the fraction of HxP from J_{3af} that does not recycle is the product of Equations 1 and 2, while the fraction which recycles (i.e., re-enters J_1 and J_{3f} such that the carbons return to the HxP pool a minimum of two times) is

$$\left(\frac{J_{3af}}{J_0 + J_{3af}}\right)^2 \quad (3)$$

From (Gebril et al., 2016), the fractional content of a given label L returning to the HxP pool via J_{3af} x times is

$${}^{x}F_{L}^{HxP} = \left(\frac{J_{3af}}{J_0 + J_{3af}}\right)^{x} \left(1 - \frac{J_{3af}}{J_0 + J_{3af}}\right) * \frac{\sum_1^m {}^{x-1}F_a^{PP} * {}^{x-1}F_b^{PP} * {}^{x-1}F_c^{PP}}{\sum_1^n {}^{x-1}F_{any}^{PP} * {}^{x-1}F_{any}^{PP} * {}^{x-1}F_{any}^{PP}} \quad (4)$$

Equation 4 is the basis for quantitatively tracking the fractional yield of each HxP label $({}^{x}F_{L}^{HxP})$ that has recycled $x-1$ times. The sum of m possible combinations of three pentose phosphate (PP) labels a, b, and c which yield HxP label L is normalized to the sum of all possible n combinations of three pentose phosphates recombining in J_{3f}. The fractional content of pentose phosphates a, b, and c from prior cycles of J_1 and J_{3f} $({}^{x-1}F_{a,b,c}^{PP})$ is determined from the previous composition of the HxP pool after taking into account the loss of carbon 1 in the oxidative PPP. Predicting the fractional M-M3 lactate is therefore partly accomplished by optimizing the flux ratio $J_{3af}/(J_0 + J_{3af})$, which determines the fractional abundance of the different HxP labels produced by recycling.

A major update to the model was accounting for ^{13}C reshuffling by reverse flux through the nonoxidative PPP to allow greater flexibility in predicting ^{13}C distribution in lactate without having to assume low nucleotide synthesis relative to oxidative PPP flux. This required

introduction of a new model-optimized flux ratio-J_{3af}/J_{3ar} (along with $J_{3af}/(J_0 + J_{3af})$, $J_7(J_{2b} + J_7)$, and J_5)- so that J_{3ar} and thus J_{3r} could be calculated. Since the model was developed to determine fluxes through reaction blocks rather than through individual reactions, ^{13}C randomization by reverse (as well as forward) flux was only considered at the level of the reaction block and the explicit metabolites (Fig. 1). Thus, reverse flux was calculated as a linked, three reaction process from HxP/TrP substrates to R5P/X5P products without considering the independent reversibility of individual reactions that could return one or more implicit metabolites in the block (i.e., E4P, S7P, G3P) to the substrate pool. Reverse flux J_{3r} affects labeling of the pentose phosphate pool (R5P and X5P) according to its contribution to the pool (vs. that of the oxidative PPP J_1) and the fractional content of the different pentose labels produced from all combinations of HxP and TrP that enter the reverse PPP. Given that J_{3r} affects labeling of the R5P/X5P pool, which in turn affects label distribution in the HxP and TrP pools as the forward (recycling) reaction occurs, it follows that changes in J_{3af}/J_{3ar} will, to some degree, affect lactate labeling provided that a significant forward flux existed.

This update required compiling R5P/X5P products resulting from all combinations of labels in the HxP and TrP pools. The fractional content of pentose phosphate label L in the pool $({}^{x}F_{L}^{PP})$ is the sum of that produced by the reverse non-oxidative PPP J_{3r} and by the oxidative PPP J_1 following the x^{th} return of HxP through J_{3af}:

$$ {}^{x}F_{L}^{PP} = \frac{\sum_1^m {}^{x}F_a^{HxP} * {}^{x}F_b^{HxP} * {}^{x}F_c^{TrP}}{\sum_1^n {}^{x}F_{any}^{HxP} * {}^{x}F_{any}^{HxP} * {}^{x}F_{any}^{TrP}} * \left(\frac{J_{3r}}{J_1+J_{3r}}\right) + ({}^{x}F_d^{HxP} + {}^{x}F_e^{HxP}) * \frac{J_1}{J_1+J_{3r}} \quad (5) $$

The first term in Eq. 5 is the sum of m combinations of HxP labels a and b, and TrP label c that together yield the specific pentose phosphate label L, normalized to the sum of all n possible combinations of HxP/TrP, adjusted for the contribution of J_{3r} to labeling the pentose phosphate pool. The second term reflects the sum of HxP labels d and e that when metabolized through J_1 yield pentose label L, adjusted for the contribution of J_1 to labeling the pentose phosphate pool. The fractional contents of the HxP labels in Eq. 5 are calculated from Eq. 4. The fractional content of TrP label derived from glycolysis (J_{2a}) and the forward pentose cycle (J_{3bf}) after x returns of HxP through J_{3af} $({}^{x}F_{L}^{TrP})$ is

$$ {}^{x}F_{L}^{TrP} = \frac{\sum_1^m \frac{{}^{x}F_a^{HxP}}{2}}{\sum_1^n {}^{x}F_{all}^{HxP}} * \frac{2J_{2a}}{2J_{2a}+J_{3bf}} + \sum_1^x \left[\frac{\sum_1^m {}^{x}F_a^{PP} * {}^{x}F_b^{PP} * F_c^{PP}}{\sum_1^n {}^{x}F_{any}^{PP} * {}^{x}F_{any}^{PP} * F_{any}^{PP}} * \left(\frac{J_{3af}}{J_0+J_{3af}}\right)^x \left(1 - \frac{J_{3af}}{J_0+J_{3af}}\right) \left(\frac{J_{3bf}}{2J_{2a}+J_{3bf}}\right) \right] \quad (6) $$

The first term in Eq. 6 reflects the fractional yield of TrP label L as m HxP labels are metabolized through J_{2a} relative to all possible n HxP labels metabolized to TrP, adjusted for the contribution of J_{2a} to labeling the TrP pool. The second term is the cumulative sum from x rounds of the pentose cycle J_{3bf} producing TrP label L from m combinations of pentose

phosphate labels *a*, *b*, and *c*, normalized to the *n* possible combinations of all pentose phosphates and adjusted for the contribution of J_{3bf} to producing TrP.

The calculations were implemented in a step-wise, serial manner (Fig. 3). To begin, the fractional content of the pentose phosphate pool was determined from the composition of the HxP pool (100% [1,2-$^{13}C_2$]HxP prior to operation of the pentose cycle) by summation of the fractional content of HxP labels that yield the same pentose phosphate label after decarboxylation of carbon 1. This was followed by applying Eq. 4 to update the HxP pool composition as the pentose phosphates recombine to return carbons to the HxP pool via J_{3af}. The TrP pool composition was then calculated with Eq. 6 from TrP generated by J_{3bf} and by processing of HxP through J_{2a}. The final step was revision of the pentose phosphate pool composition from J_{3r} using Eq. 5. The calculations were repeated for six rounds of HxP recycling to obtain the 'final' pentose phosphate, HxP, and TrP pool compositions, from which pyruvate/lactate labeling was determined. Inclusion of reverse PPP flux substantially increased the scope of calculations, as it required tracking the abundance of 32 pentose phosphate, 8 TrP, and 64 HxP labels after two rounds of recycling. All subsequent rounds of forward and reverse flux calculations required accounting for 32,768 possible combinations of substrates (32^3 as three pentose phosphates recombine in J_{3f}; $64^2\times8$ as two HxP and 1 TrP recombine in J_{3r}), which substantially lengthened the time required to complete the calculations.

^{13}C distribution in the pentose phosphates, HxP, and lactate was assessed over a broad range for J_{3af}/J_{3ar} (from 10^5, essentially unidirectional forward non-oxidative PPP flux, to 0.55, the minimum possible assuming $J_{3af}/(J_0 + J_{3af})$ = 0–25) to gauge the effect of reverse PPP flux in the model. Interestingly reverse flux substantially changed R5P/X5P labeling but only modestly affected the HxP pool (Table 1). Consequently, lactate M2 and M3 were modestly enriched by a maximum of 1.55 and 0.95%, respectively at the expense of M (−1.89%) and M1 (−0.60%) when the forward non-oxidative PPP accounted for 25% labeling of the HxP pool (Fig. 4). These results are consistent with the model developed by (KATZ and Rognstad, 1967) who found that reverse flux affected labeling of the pentose phosphates more than the HxPs, and had relatively minor effects on ^{14}C distribution in lactate. Note that the influence reverse flux has on ^{13}C distribution in the HxP pool (and thus lactate) will diminish as the forward non-oxidative PPP flux decreases (i.e., decreased $J_{3af}/(J_0 + J_{3af})$). It is also worth noting that because J_{3af} appears in two solver-optimized ratios, they are not independent of one another. This dependency was evaluated by determining the upper limit to $J_{3af}/(J_0 + J_{3af})$ over a range of values for J_{3af}/J_{3ar} (Fig. 5). When the latter ratio was less than 1, the upper limit of $J_{3af}/(J_0 + J_{3af})$ was constrained by the requirement that $J_1 \geq 0$. This constraint arose to satisfy the required steady-state for the HxP pool:

$$J_0+J_{3af}=J_1+J_{3ar}+J_{2a} \quad (7)$$

Conversely, when $J_{3af}/J_{3ar} > 1$, the upper limit to $J_{3af}/(J_0 + J_{3af})$ was constrained by the requirement that $J_9 \geq 0$ to satisfy the steady-state for the R5P/X5P pool:

$$J_1 + J_{3r} = J_{3f} + J_9 \quad (8)$$

As J_{3af}/J_{3ar} approaches unity, it is possible for $J_{3af}/(J_0 + J_{3af})$ to approach 0.9999, but the calculated labeling pattern in lactate will accurately reflect that produced by cells given that $J_{3af} \gg J_1$ and J_{2a}. After six rounds of recycling, less than 0.1% of the HxP that recycles would have left the HxP pool via glycolysis and the pentose cycle, and thus the final M-M3 lactate would reflect less than 0.1% of what should be produced. Practically, $J_{3af}/(J_0 + J_{3af})$ should be ≤0.60 to minimally account for 98% of recycled HxP. Despite the greater time necessary for computations, accounting for J_{3r} allows for greater applicability of the model to cells or conditions where demand for pentose phosphates for nucleotide synthesis might exceed the demand for NADPH.

3.1.4. Qualitative and quantitative ^{13}C rearrangements in the TCA cycle—Malic enzyme produces pyruvate and NADPH from oxidation of malate, which is assumed to be derived exclusively from the TCA cycle. Therefore a fraction of cytoplasmic pyruvate contains 'recycled' ^{13}C that has been subjected to reshuffling within the TCA cycle (Fig. 6). The original model quantitated malate labeling through four turns of the TCA cycle as ^{13}C in pyruvate entered the cycle, but neglected to consider that succinate dehydrogenase cannot distinguish between the two carboxylic acids in succinate due to its symmetry. With the exception of unlabeled succinate, or label at positions 1,4, 2,3, or 1,2,3,4, each (of twelve possible) succinate label will be metabolized such that the ^{13}C position in half of the malate will be inverted relative to the label position in succinate (e.g., for ^{13}C at carbons 1 and 2 in succinate, 50% of the resulting malate will be labeled at positions 1,2 and 50% labeled at positions 3,4; Fig. 6). This doubles the number of unique malate labels in the first two turns of the cycle compared to the labels reported in Table 2 of (Gebril et al., 2016). Quantitative tracking of each label for turn x of the TCA cycle was determined essentially as previously described except that the yield of malate label L (that also has an inverse label; i.e., L= 1, 2, 3, 4, 1,2, 3,4, 1,3, 2,4, 1,2,3, 2,3,4, 1,2,4, and 1,3,4) from the sum of all m combinations of pyruvate label a and malate label b (after conversion to acetyl CoA and oxaloacetate, respectively) is half of that shown in Table 2 of Gebril et al (2016)

$$^{x}F_{L}^{Mal} = \sum_{1}^{m} \frac{^{x-1}F_{a}^{Mal} * F_{b}^{Pyr}}{2} \quad (9)$$

By inclusion of the additional ^{13}C reshuffling by succinate dehydrogenase, it was found that seven turns of the TCA cycle were necessary for malate to approach an isotopic steady state compared to the four turns in the previous model. This update substantially increased M1 and M2 pyruvate from malic enzyme while reducing M and M3 pyruvate, but the effect on exported lactate was more modest and depended on the contribution of J_7 to the pyruvate pool (Table 2).

3.2. Flux calculations

The ten fluxes not measured (Fig. 1; J_1,J_{2a},J_{2b},J_{3f},J_{3r},J_5,J_6,J_7,J_8,J_9) can be determined from J_0,J_4,J_{RR}, and M-M3 lactate provided the cells maintain a metabolic steady-state over the experiment. Five of the unknown fluxes (J_{3f},J_{3r},J_5,J_6,J_7) are determined from the measured variables in the following manner. Assume the model reproduces M-M3 lactate with $J_{3af}/(J_0 + J_{3af}) = X$, $J_{3af}/J_{3ar} = Y$ and $J_7/(J_{2b} + J_7) = Z$, then $J_{3af} = X * J_0/(1-X)$ and $J_{3ar} = J_{3af}/Y$ (units of F6P produced or consumed/min, respectively). By stoichiometry, the remaining non-oxidative PPP fluxes are: $J_{3f} = 1.5 * J_{3af}$ (units of pentose phosphate consumed/min), $J_{3bf} = J_{3f}/3$ (units of TrP produced/min), $J_{3r} = 1.5 * J_{3ar}$ (units of pentose phosphate produced/min), and $J_{3br} = J_{3r}/3$ (units of TrP consumed/min). Concurrently, mitochondrial pyruvate oxidation J_5 is optimized within the stoichiometric constraints that $J_{Tr} = 5 * J_5 + J_6$ and $J_5 \geq J_6$. Malic enzyme flux is determined as $J_7 = Z * (J_4 + J_5)$ since, from the steady-state pyruvate level, $J_{2b} + J_7 = J_4 + J_5$. Furthermore since pyruvate and NADH are both derived from J_{2b}, it is apparent from the pyruvate steady-state that production of glycolytic NADH (and pyruvate) decreases as ME flux increases, so $J_6 = J_5 - J_7$ given a constant NADH consumption by J_4. The remaining five fluxes can be calculated from the steady-state and reaction stoichiometries: $J_{2b} = J_4 + J_5 - J_7$, $J_{2a} = 0.5 * (J_{2b} - J_{3bf})$, $J_1 = J_0 + J_{3af} - J_{2a} - J_{3ar}$, $J_8 = 2 * J_1 + J_7$, and $J_9 = J_1 + J_{3r} - J_{3f}$. In this way four measured variables can be sufficient to obtain substantial quantitative information on glucose utilization.

3.3. Application of the model

3.3.1. Re-evaluating ^{13}C distribution in lactate from metabolism of [1,2-$^{13}C_2$]glucose—

As the updated model was evaluated, it became apparent that quantitation of M-M3 lactate was necessary to reach a single, ‘global’ solution, as multiple ‘local’ solutions were possible if the small contribution of M3 lactate was excluded as in (Gebril et al., 2016). This, together with the inability of the updated model to adequately reproduce M-M2 lactate measured previously by LC QTOF MS/MS, necessitated re-analysis of ^{13}C distribution in lactate from CGNs. Closer inspection of the MS/MS data reported in (Gebril et al., 2016) revealed that the derivatized ions were not completely separated by QTOF prior to quantitation of the fragments. Unlabeled lactate (M=224 Da peak) contained 225 (M1) and 226 (M2) Da ions, and, similarly, the 225 Da (M1) peak contained 226 Da (M2) ions. This revelation invalidated the fractional ^{13}C distribution previously reported (Gebril et al., 2016), as quantification of the 152 Da fragment from each peak was cross-contaminated with fragments from the higher molecular weight ions. Triple quadrupole mass spectrometry (LC-TQMS) was found superior to QTOF-MS/MS for both separating and detecting the ions. From analysis of M and M1 (3-^{13}C lactate from Cambridge Isotope Laboratories) standards, 96.7±0.3% and 96.3±0.2% of lactate was found in their respective 224 and 225 Da peaks (Table 3). Importantly, Cambridge Isotope lot analysis reported 1.5% residual unlabeled lactate in the M1 standard (i.e., 224 Da when derivatized), which agreed well with the current LC-TQMS results of 1.3±0.3%. If the 225 Da ion had cross-contaminated the 224 Da peak, then a much greater percentage of unlabeled lactate would be expected for the M1 standard. Endogenous ^{13}C present as M1 in the ^{12}C lactate standards averaged 2.87±0.24%, which was similar to 3.35±0.10% endogenous M1 lactate observed in neurons metabolizing ^{12}C glucose. Further evidence

suggesting separation of M and M1 was from LC-TQMS analysis of 7.65:1 M:M1 mixed standards, which yielded a 6.91±0.08:1 ratio (n=5 different concentrations from 100–800 μM). With this method, M3 lactate was reliably detected above background for cells metabolizing [1,2-$^{13}C_2$]glucose and found to constitute 1.19±0.04% of total lactate. As expected, M1 lactate was less abundant than previously measured since cross contamination with M2 was eliminated, but remarkably M1 accounted for only 2.49±0.07% of total lactate (vs. 18.6% measured previously). Thus, this more careful analysis, which supersedes that reported in (Gebril et al., 2016), yielded a substantially different lactate labeling pattern (Table 3) for use in the revised model.

3.3.2. Updated assessment of metabolic fluxes and pentose cycle activity in cultured neurons—Cerebellar granule neuron fluxes J_0, J_4, and J_{RR} (where RR denotes mitochondrial respiration rate) measured previously with [^{12}C]glucose as the sole substrate (n=6) (Gebril et al., 2016) were used with the revised model to solve for the unknown fluxes by optimizing J_{3af}/J_{3ar}, $J_{3af}/(J_0 + J_{3af})$, $J_7/(2J_{2a} + J_{3bf} + J_7)$, and J_5 to reproduce the re-measured fractional M-M3 lactate (n=5 for neurons using [1,2-$^{13}C_2$]glucose as sole substrate) reported in Table 3. However, the model was unable to reproduce the average M-M3 lactate pattern (Table 4). As a result, the unknown fluxes were estimated by minimizing the summed difference (i.e., error) between the predicted M-M3 pattern $(M_i^{Predict})$ and the measured M-M3 pattern $(M_i^{Measured})$:

$$\sum_{i=0}^{3} \left| M_i^{Predict} - M_i^{Measured} \right| = minimum \quad (10)$$

It was not surprising that, for all experiments, the model was constrained (by the requirement that $J_{3af}/(J_0 + J_{3af}) \geq 0.00001$) to the same solution given that M-M3 lactate was measured from separate experiments (Table 4). Monte Carlo simulations conducted as in (Gebril et al., 2016) provided an estimate of the additional variation in fluxes to be expected for simultaneous measurements of M-M3 lactate and J_0, J_4, and J_{RR} (Table 4, minimum and maximum from the simulations designated in parentheses below each mean). Most of the error was associated with underestimating M2 lactate and correspondingly overestimating M3 lactate.

The most important result from this new analysis was negligible forward non-oxidative PPP flux, and thus no apparent pentose cycle activity or recycling of hexose phosphates from the non-oxidative PPP into the oxidative PPP. The forward flux was designated negligible rather than zero for validity of the calculations (hence the constraint $J_{3af}/(J_0 + J_{3af}) \geq 0.00001$). Thus, in cultured CGNs from newborn rats with depolarizing levels of extracellular K^+ (25mM), effectively none of the glucose taken up was consumed by the pentose cycle (although up to 39% of glucose was consumed by the oxidative PPP and reactions synthesizing nucleotides- see below). This result contrasts with our previous data suggesting the pentose cycle consumed 19.5% of glucose, and is consistent with other reports also evaluating isotope distribution in lactate (Ben-Yoseph et al., 1996; Brekke et al., 2012) that have demonstrated very low basal pentose cycle activity (0–4% of total glucose consumption) in cultured neurons. In such cases of minimal pentose cycle activity, the

difference in flux estimation should be small for HxP recycling and non-recycling models. The differences between models are expected to be more substantial for *in vivo* brain metabolism experiments, glial cell enriched cultures, or oxidatively stressed neuronal cultures where apparent pentose cycle activity consumes from 4–15% (unstressed cultured glial cells; neonatal or adult brain) to 25–40% (stressed neurons) of total glucose (Amaral et al., 2011; Amaral et al., 2016; Ben-Yoseph et al., 1995; Ben-Yoseph et al., 1996; Brekke et al., 2014; Dusick et al., 2007; Morken et al., 2014), in which case accounting for HxP recycling becomes more important. Since the unstressed CGNs in this study exhibited negligible pentose cycle flux, ^{13}C reshuffling by the TCA cycle and malic enzyme largely explained the deviation in lactate labeling from 50% M/M2 expected by glycolysis. The results suggest approximately 7.8% of pyruvate was derived from malic enzyme, which is consistent with what we reported previously (Gebril et al., 2016) despite incomplete assessment of TCA cycle ^{13}C randomization in the original model. This is also similar to malic enzyme in cultured astrocytes which was responsible for producing 5% of total pyruvate (Amaral et al., 2011). The fact that the model did not exactly reproduce M-M3 lactate could indicate that (1) isotopic steady-states may not have been reached in the glutamate and/or aspartate pools that are subject to transaminase exchange reactions with TCA cycle α-ketoglutarate and oxaloacetate pools, respectively, (2) contaminating glial cells may have supplied alternatively labeled substrates (e.g., glutamine, pyruvate) that affected ^{13}C distribution in the relevant neuronal metabolite pools (e.g., α-ketoglutarate, pyruvate), (3) differentially labeled pyruvate pools (from incomplete mixing of pyruvate from glycolysis, malic enzyme, and/or the pentose cycle) may have been preferentially channeled to either mitochondria or lactate dehydrogenase, and/or (4) significant reverse flux through malic enzyme may have affected TCA cycle malate labeling by fixation of unlabeled CO_2. Nonetheless, the small error between measured and predicted M-M3 lactate suggests that the underlying assumptions, constraints, and system structure reasonably reflect the metabolic behavior of neurons.

With negligible forward non-oxidative PPP flux, J_{3af}/J_{3ar} became irrelevant to influencing labeling of the HxP and TrP pools and thus exported lactate, so this ratio could not be optimized in these experiments. As a result, the input data were insufficient to conclusively infer J_{3ar}, J_1, J_{2a}, J_8, and J_9 given that the proportion of glucose consumed by the oxidative PPP vs. the reverse non-oxidative PPP could not be distinguished. If J_{3r} is negligible (i.e., assume $J_{3af}/J_{3ar}= 1$; flux set 1 Table 4), then all glucose not exported as lactate nor oxidized by mitochondria (39%), would be consumed by the oxidative PPP and used subsequently for nucleotide synthesis. In this case, the upper limit to J_1 would be 112±24 pmol G6P consumed/min × 10^6 cells, which would correspond to lower limits for J_9 (112±24 pmol R5P consumed/min × 10^6 cells) and J_{2a} (178±23 pmol G6P consumed/min × 10^6 cells). At the other extreme, if the extra glucose not exported as lactate nor oxidized by mitochondria is consumed by the reverse non-oxidative PPP (flux set 2, Table 4), then J_4 would be negligible and the upper limit to J_{3r} = 135±30 pmol pentose phosphates produced/min × 10^6 cells, which in turn yields upper limits to J_{2a} (201±21 pmol G6P/min × 10^6 cells) and J_9 (135±30 pmol R5P/min × 10^6 cells). For maximal J_1 and negligible J_{3r}, the pentose phosphate pool should be 100% M1; in contrast, the predicted ^{13}C distribution with negligible J_1 and maximal J_{3r} is M=0.3333, M2=0.5000, and M4=0.1667. Thus, with

negligible forward non-oxidative PPP flux, measurement of fractional M-M5 content of the pentose phosphate pool would provide the constraints necessary to optimize J_{3af}/J_{3ar} to accurately assess J_1 and J_{3r}. In either case, the substantial percentage of glucose used for nucleotide synthesis is surprising and may be related to the young age of these neurons (isolated from P7 neonatal rats; see below).

It is likely that the true CGN fluxes are closer to set 1 than set 2 given the critical role of the oxidative PPP in NADPH synthesis/antioxidant defenses and neuronal viability (Chinta et al., 2007; Dunn et al., 2014; Fernandez-Fernandez et al., 2012; Filosa et al., 2003; Herrero-Mendez et al., 2009; Levonen et al., 2014; Li et al., 2014). Assuming negligible reverse non-oxidative PPP flux, then 39% of glucose consumption could be attributed to the oxidative PPP and the downstream reactions involved in *de novo* nucleotide synthesis (vs 61% to glycolysis) despite negligible pentose cycle activity. In this state, 7% of glucose would be lost as CO_2 in the oxidative PPP, and 32% converted to pentose phosphates for use in nucleotide synthesis. The upper limit to oxidative PPP flux is less than half of that reported previously (Gebril et al., 2016), but nonetheless suggests that up to 88% of NADPH is from J_1 vs. 12% from malic enzyme. Of course since J_{3r} might consume some of the glucose, it will be necessary to test this ‘upper limit’ of oxidative PPP glucose consumption by analysis of ^{13}C distribution in the pentose phosphates.

For glucose consumed by glycolysis, 45% was exported as lactate while the remaining 16% was oxidized by mitochondria. Hence 84% of glucose consumption was independent of mitochondrial respiration, with aerobic glycolysis accounting for the majority (54%) of this. As discussed previously (Gebril et al., 2016), the high non-mitochondrial glucose use (particularly by aerobic glycolysis) may partly be attributable to the *in vitro* culture conditions (10 mM glucose, no exogenous lactate or amino acids). However, some of the oxygen-independent glucose use may be physiologically relevant and associated with the early age of neurons in this study (isolated from 7 day old Wistar rats). A meta-analysis demonstrated that human whole brain oxygen-independent glucose consumption peaked in early childhood (approximately 5 years old) and accounted for about one-third of total glucose consumption (Goyal et al., 2014). Such use was correlated with high rates of neuronal growth, maturation, synapse formation, and/or plasticity and thus may be important for brain development. In this study, the extent to which aerobic glycolysis (45% of total glucose) vs. the oxidative PPP (up to 39% of total glucose) may be important for these processes is unknown. Nonetheless, the high rate of non-mitochondrial glucose consumption of these relatively immature neurons may partly reflect ongoing *in vitro* growth/maturation.

4. Summary and conclusions

Fluxes through the major glucose consuming reactions have been re-assessed in cerebellar granule neurons metabolizing [1,2-$^{13}C_2$]glucose using an updated model originally described in (Gebril et al., 2016) and new measurements of ^{13}C lactate labeling by triple quadrupole mass spectrometry. The updates increased the applicability of the model to different cell types by considering the reversible nature of the non-oxidative PPP, and increased the reliability of quantitatively tracking ^{13}C distribution in malate by accounting for symmetrical succinate oxidation within the TCA cycle. Reverse flux through the non-

oxidative PPP had relatively minor effects on ^{13}C distribution in the hexose phosphate pool and by extension in lactate, but this depended on the contribution of the forward non-oxidative PPP flux to labeling the HxP pool. The effect of symmetrical succinate metabolism was such that pyruvate produced by malic enzyme was predicted to have substantially greater M1/M2 and less M/M3 content, which in turn affected ^{13}C distribution in lactate according to the contribution of malic enzyme vs. glycolysis to labeling the pyruvate pool. When applied to ^{13}C lactate from cultured CGNs, the error-minimized solution indicated negligible pentose cycle activity but highly active oxidative PPP and/or reverse non-oxidative PPP flux that consumed 39% of glucose. Malic enzyme and glycolysis were responsible for 7.8 and 92.2% of pyruvate production, respectively, and largely accounted for ^{13}C labeling in exported lactate. The majority (74%) of glucose used by glycolysis was exported as lactate as opposed to oxidized by mitochondria. The high mitochondrial-independent glucose utilization may be a consequence of the young age of neurons as well as the *in vitro* conditions used. The current approach offers a few advantages compared to other models that evaluate fluxes from ^{13}C labeling in glycolytic and/or TCA cycle metabolites by (1) providing more accurate estimations of pentose cycle activity for redox homeostasis by accounting for HxP recycling and reverse non-oxidative PPP flux, particularly in situations where the cycle becomes a significant glucose consumer (e.g., in stressed neurons, glial cells, or the intact brain), (2) quantifying glucose utilization by the oxidative PPP for both redox homeostasis and provision of pentose phosphates used for nucleotide synthesis, a flux not typically evaluated with the pentose cycle, (3) considering the affect that malic enzyme has on lactate labeling, and (4) requiring relatively few experiments for quantifying fluxes through all major glucose consuming reactions.

Acknowledgments

Funding Information

This work was supported by Grant No. 1R15CA199016-01A1 from the National Cancer Institute. The NIH had no role in the design, execution, interpretation, and reporting of the experiments described herein.

Abbreviations list

PPP	pentose phosphate pathway
LC-MS/MS	liquid chromatography tandem mass spectrometry
LC-TQ-MS	liquid chromatography triple quadrupole mass spectrometry
LC-QTOF	liquid chromatography quadrupole time of flight mass spectrometry
HxP	hexose phosphate (referring to both glucose-6-phosphate and fructose-6-phosphate)
G6P	glucose-6-phosphate
F6P	fructose-6-phosphate
TrP	triose phosphates (referring to both dihydroxyacetone phosphate and glyceraldehyde-3-phosphate)

G3P	glyceraldehyde-3-phosphate
R5P	ribose-5-phosphate
X5P	xyulose-5-phosphate
Ri5P	ribulose-5-phosphate
TCA	tricarboxylic acid
M	a metabolite having no ^{13}C atoms derived from [1,2-$^{13}C_2$]glucose
M1	a metabolite having one ^{13}C atom derived from [1,2-$^{13}C_2$]glucose
M2	a metabolite having two ^{13}C atoms derived from [1,2-$^{13}C_2$]glucose
M3	a metabolite having three ^{13}C atoms derived from [1,2-$^{13}C_2$]glucose
J_x	flux through reaction x

References

Ainscow EK, Brand MD. Top-down control analysis of ATP turnover, glycolysis and oxidative phosphorylation in rat hepatocytes. Eur J Biochem. 1999:671–685.

Amaral AI, Hadera MG, Tavares JM, Kotter MR, Sonnewald U. Characterization of glucose-related metabolic pathways in differentiated rat oligodendrocyte lineage cells. Glia. 2016:21–34. [PubMed: 26352325]

Amaral AI, Teixeira AP, Hakonsen BI, Sonnewald U, Alves PM. A comprehensive metabolic profile of cultured astrocytes using isotopic transient metabolic flux analysis and C-labeled glucose. Front Neuroenergetics. 2011:5. [PubMed: 21941478]

Belanger M, Allaman I, Magistretti PJ. Brain energy metabolism: focus on astrocyte-neuron metabolic cooperation. Cell Metab. 2011:724–738. [PubMed: 22152301]

Ben-Yoseph O, Boxer PA, Ross BD. Assessment of the role of the glutathione and pentose phosphate pathways in the protection of primary cerebrocortical cultures from oxidative stress. J Neurochem. 1996:2329–2337. [PubMed: 8632155]

Ben-Yoseph O, Camp DM, Robinson TE, Ross BD. Dynamic measurements of cerebral pentose phosphate pathway activity in vivo using [1,6,13C2,6,6-2H2]glucose and microdialysis. J Neurochem. 1995:1336–1342. [PubMed: 7861166]

Boyle PJ, Scott JC, Krentz AJ, Nagy RJ, Comstock E, Hoffman C. Diminished brain glucose metabolism is a significant determinant for falling rates of systemic glucose utilization during sleep in normal humans. J Clin Invest. 1994:529–535. [PubMed: 8113391]

Brekke EM, Morken TS, Wideroe M, Haberg AK, Brubakk AM, Sonnewald U. The pentose phosphate pathway and pyruvate carboxylation after neonatal hypoxic-ischemic brain injury. J Cereb Blood Flow Metab. 2014:724–734. [PubMed: 24496178]

Brekke EM, Walls AB, Schousboe A, Waagepetersen HS, Sonnewald U. Quantitative importance of the pentose phosphate pathway determined by incorporation of 13C from [2-13C]- and [3-13C]glucose into TCA cycle intermediates and neurotransmitter amino acids in functionally intact neurons. J Cereb Blood Flow Metab. 2012:1788–1799. [PubMed: 22714050]

Chinta SJ, Kumar MJ, Hsu M, Rajagopalan S, Kaur D, Rane A, Nicholls DG, Choi J, Andersen JK. Inducible alterations of glutathione levels in adult dopaminergic midbrain neurons result in nigrostriatal degeneration. J Neurosci. 2007:13997–14006. [PubMed: 18094238]

Dienel GA, Cruz NF. Aerobic glycolysis during brain activation: adrenergic regulation and influence of norepinephrine on astrocytic metabolism. J Neurochem. 2016:14–52. [PubMed: 27166428]

Dunn L, Allen GF, Mamais A, Ling H, Li A, Duberley KE, Hargreaves IP, Pope S, Holton JL, Lees A, Heales SJ, Bandopadhyay R. Dysregulation of glucose metabolism is an early event in sporadic Parkinson's disease. Neurobiol Aging. 2014:1111–1115. [PubMed: 24300239]

Dusick JR, Glenn TC, Lee WN, Vespa PM, Kelly DF, Lee SM, Hovda DA, Martin NA. Increased pentose phosphate pathway flux after clinical traumatic brain injury: a [1,2-13C2]glucose labeling study in humans. J Cereb Blood Flow Metab. 2007:1593–1602. [PubMed: 17293841]

Fernandez-Fernandez S, Almeida A, Bolanos JP. Antioxidant and bioenergetic coupling between neurons and astrocytes. Biochem J. 2012:3–11. [PubMed: 22417747]

Filosa S, Fico A, Paglialunga F, Balestrieri M, Crooke A, Verde P, Abrescia P, Bautista JM, Martini G. Failure to increase glucose consumption through the pentose-phosphate pathway results in the death of glucose-6-phosphate dehydrogenase gene-deleted mouse embryonic stem cells subjected to oxidative stress. Biochem J. 2003:935–943. [PubMed: 12466018]

Gebril HM, Avula B, Wang YH, Khan IA, Jekabsons MB. (13)C metabolic flux analysis in neurons utilizing a model that accounts for hexose phosphate recycling within the pentose phosphate pathway. Neurochem Int. 2016:26–39.

Goyal MS, Hawrylycz M, Miller JA, Snyder AZ, Raichle ME. Aerobic glycolysis in the human brain is associated with development and neotenous gene expression. Cell Metab. 2014:49–57. [PubMed: 24411938]

Herrero-Mendez A, Almeida A, Fernandez E, Maestre C, Moncada S, Bolanos JP. The bioenergetic and antioxidant status of neurons is controlled by continuous degradation of a key glycolytic enzyme by APC/C-Cdh1. Nat Cell Biol. 2009:747–752. [PubMed: 19448625]

KATZ J, Rognstad R. The labeling of pentose phosphate from glucose-14C and estimation of the rates of transaldolase, transketolase, the contribution of the pentose cycle, and ribose phosphate synthesis. Biochemistry. 1967:2227–2247. [PubMed: 6049456]

Kochetov GA, Solovjeva ON. Structure and functioning mechanism of transketolase. Biochim Biophys Acta. 2014:1608–1618.

Levonen AL, Hill BG, Kansanen E, Zhang J, Darley-Usmar VM. Redox regulation of antioxidants, autophagy, and the response to stress: implications for electrophile therapeutics. Free Radic Biol Med. 2014:196–207.

Li M, Sun M, Cao L, Gu JH, Ge J, Chen J, Han R, Qin YY, Zhou ZP, Ding Y, Qin ZH. A TIGAR-regulated metabolic pathway is critical for protection of brain ischemia. J Neurosci. 2014:7458–7471. [PubMed: 24872551]

Madsen PL, Hasselbalch SG, Hagemann LP, Olsen KS, Bulow J, Holm S, Wildschiodtz G, Paulson OB, Lassen NA. Persistent resetting of the cerebral oxygen/glucose uptake ratio by brain activation: evidence obtained with the Kety-Schmidt technique. J Cereb Blood Flow Metab. 1995:485–491. [PubMed: 7714007]

McKenna, MC., Dienel, GA., Sonnewald, U., Waagepetersen, HS., Schousboe, A. Energy Metabolism of the Brain, in Basic Neurochemistry. In: Brady, ST.Siegel, GJ.Albers, RW., Price, DL., editors. Principles of Molecular, Cellular, and Medical Neurobiology. 8th. Elsevier; 2012. p. 200-231.

McKenna MC, Stevenson JH, Huang X, Tildon JT, Zielke CL, Hopkins IB. Mitochondrial malic enzyme activity is much higher in mitochondria from cortical synaptic terminals compared with mitochondria from primary cultures of cortical neurons or cerebellar granule cells. Neurochem Int. 2000:451–459. [PubMed: 10733013]

Morken TS, Brekke E, Haberg A, Wideroe M, Brubakk AM, Sonnewald U. Neuron-astrocyte interactions, pyruvate carboxylation and the pentose phosphate pathway in the neonatal rat brain. Neurochem Res. 2014:556–569. [PubMed: 23504293]

Samland AK, Sprenger GA. Transaldolase: from biochemistry to human disease. Int J Biochem Cell Biol. 2009:1482–1494. [PubMed: 19401148]

Settergren G, Lindblad BS, Persson B. Cerebral blood flow and exchange of oxygen, glucose, ketone bodies, lactate, pyruvate and amino acids in infants. Acta Paediatr Scand. 1976:343–353. [PubMed: 5840]

Vaishnavi SN, Vlassenko AG, Rundle MM, Snyder AZ, Mintun MA, Raichle ME. Regional aerobic glycolysis in the human brain. Proc Natl Acad Sci USA. 2010:17757–17762. [PubMed: 20837536]

WOOD HG, KATZ J. The distribution of C14 in the hexose phosphates and the effect of recycling in the pentose cycle. J Biol Chem. 1958:1279–1282. [PubMed: 13610827]

Zwingmann, C., Leibfritz, D. Glial-Neuronal Shuttle Systems, in Brain Energetics. In: Gibson, GE., Dienel, GA., editors. Integration of Molecular and Cellular Processes. 3rd. Springer; 2007. p. 197-238.

Highlights

- Reverse non-oxidative PPP flux was incorporated in a ^{13}C metabolic flux model.
- The model was applied to cerebellar granule neurons from neonatal rat brains.
- The oxidative and reverse non-oxidative PPP consumed 39% of the glucose.
- Glucose consumption by the pentose cycle was negligible.
- The updated model offers advantages to assessing pathway fluxes.

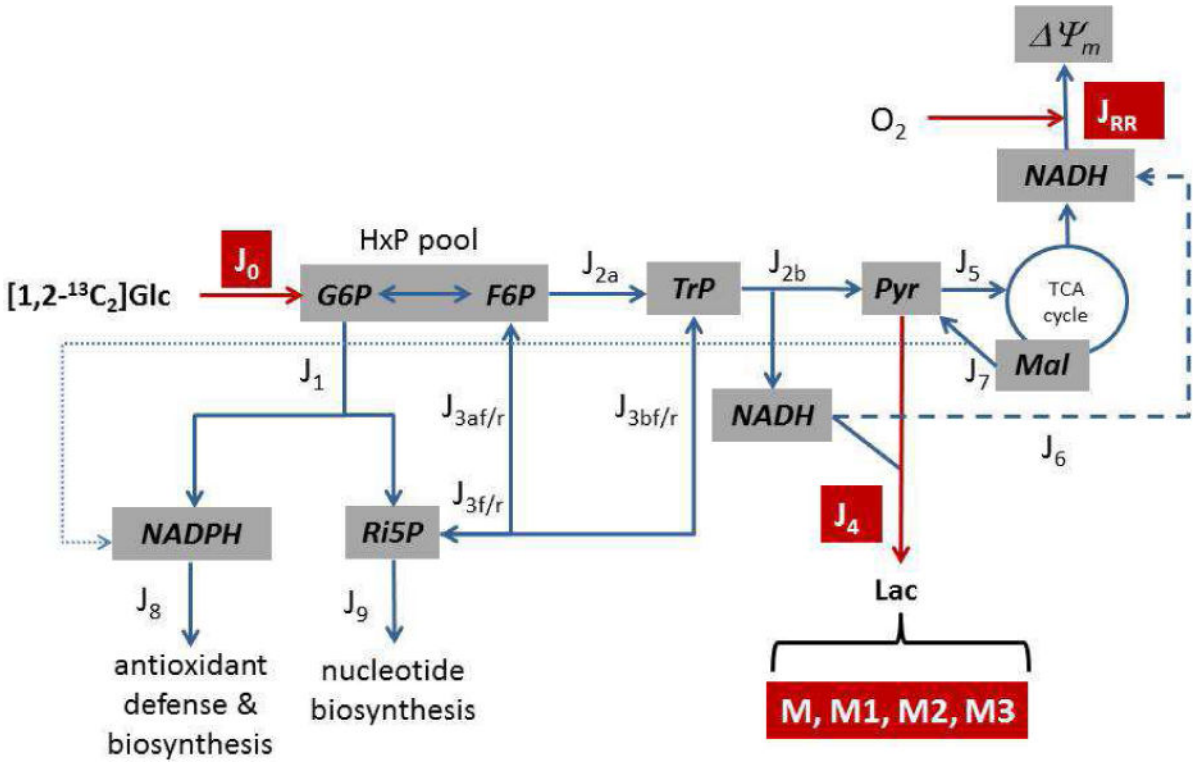

Figure 1.

Organization of glucose metabolism into reaction blocks for ^{13}C metabolic flux analysis. Measured fluxes (red) include glucose uptake and phosphorylation (J_0), lactate production and export (J_4), and mitochondrial respiration rate (J_{RR}). Metabolism of [1,2-$^{13}C_2$]glucose yields lactate (Lac) whose enrichment with one (M1), two (M2), or three (M3) ^{13}C atoms depends on fluxes through the oxidative pentose phosphate pathway (PPP; J_1), the forward non-oxidative PPP (J_{3f},J_{3af},J_{3bf}) that consumes ribulose-5-phosphate (Ri5P) and produces hexose phosphates (HxP; G6P, glucose-6-phosphate; F6P, fructose-6-phosphate) and triose phosphates (TrP; dihydroxyacetone phosphate and glyceraldehyde-3-phosphate), the reverse non-oxidative PPP (J_{3r},J_{3ar},J_{3br}), glycolysis (J_{2a}, J_{2b}, which produce and consume TrP, respectively), mitochondrial pyruvate (Pyr) oxidation (J_5), and oxidation of mitochondrial malate (Mal; J_7) by malic enzyme. All fluxes can be inferred from ^{13}C enrichment in lactate by predicting the relative yield of ^{13}C-enriched products from each reaction. Accurately predicting M-M3 lactate is achieved by optimizing $J_{3af}/(J_0 + J_{3af})$, $J_7/(J_{2b} + J_7)$. J_{3af}/J_{3ar}, and J_5. Consumption of NADPH (J_8), Ri5P for nucleotides (J_9), and glycolytic NADH by mitochondria (J_6) are 'balance' fluxes calculated from the inferred and measured fluxes that do not directly influence ^{13}C enrichment in lactate.

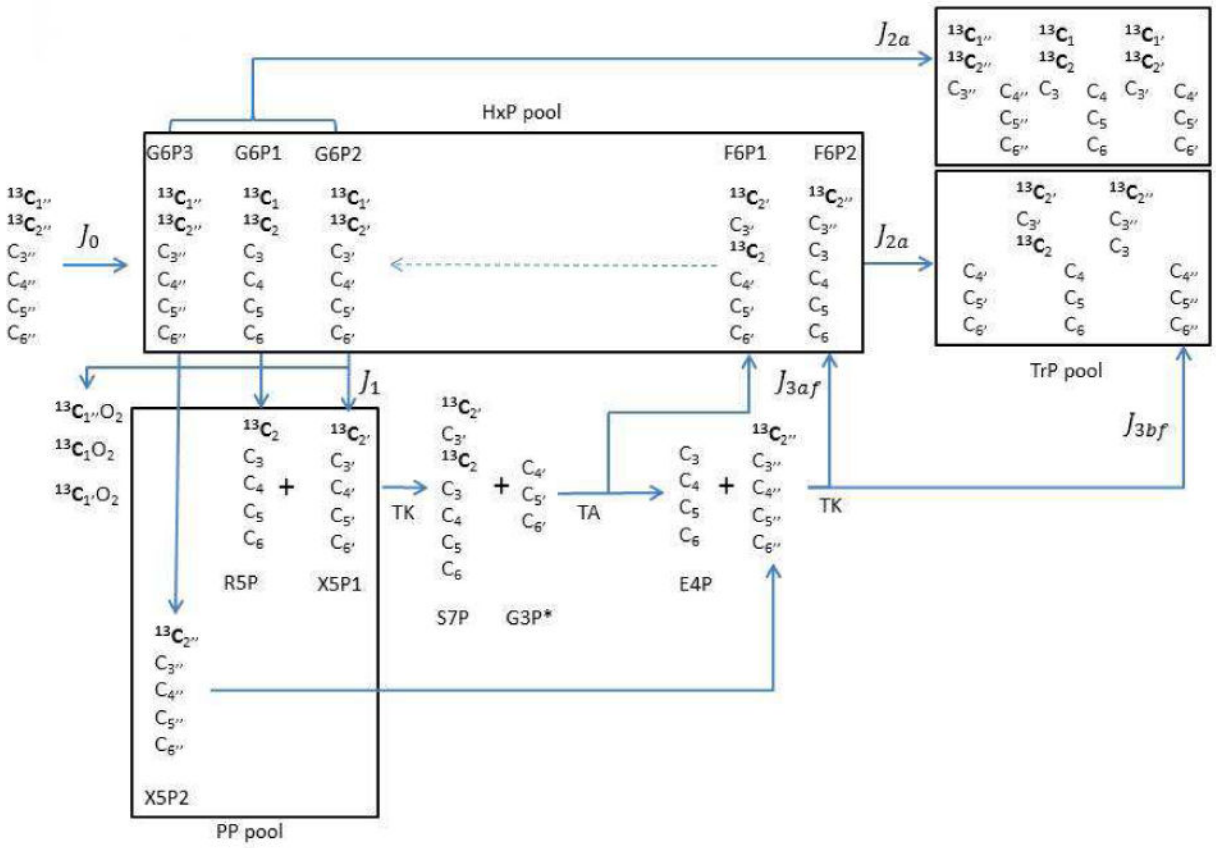

Figure 2.

Carbon reshuffling in the pentose phosphate pathway. The hexose phosphate (HxP), pentose phosphate (PP), and triose phosphate (TrP) pools (boxed) are connected by the oxidative and non-oxidative PPP, and glycolysis. Carbon atoms from three glucose-6-phosphates (G6P1-3) derived from exogenous [1,2-$^{13}C_2$]glucose via J_0 are distinguished with subscripts (C_x, $C_{x'}$, $C_{x''}$, where x=1–6) that reflect their original positions in G6P. Only C_1–C_3 of the original G6P entering the pentose cycle are reshuffled in fructose-6-phosphate (F6P) as ribose-5-phosphate (R5P) and xylulose-5-phosphate (X5P) return to the HxP pool in the forward non-oxidative PPP (J_{3f} and J_{3af} reflect the rates of pentose phosphate consumption and F6P production, respectively, by the forward non-oxidative PPP) by transketolase (TK) and transaldolase (TA). The fraction of returning F6P that equilibrates with G6P and recycles through J_1 and J_{3af} to return to the HxP pool at least twice is modeled as $[J_{3af}/(J_0 + J_{3af})]^2$ while the fraction that does not recycle is $(J_{3af}/(J_0 + J_{3af}))*(1-[J_{3af}/(J_0 + J_{3af})])$. Further rounds of recycling produce a total of eight different HxP labels (unlabeled, and ^{13}C at positions 1, 2, 3, 1,2, 1,3, 2,3, and 1,2,3). Phosphofructokinase, aldolase, and triose phosphate isomerase (collectively 'upper' glycolysis J_{2a}) together with non-oxidative PPP triose phosphate (TrP) production (J_{3bf}) dictate label distribution within the glycolytic TrP pool. In the model, glyceraldehyde-3-phosphate (G3P*) generated by the first forward transketolase reaction is assumed to not equilibrate with the glycolytic TrP pool.

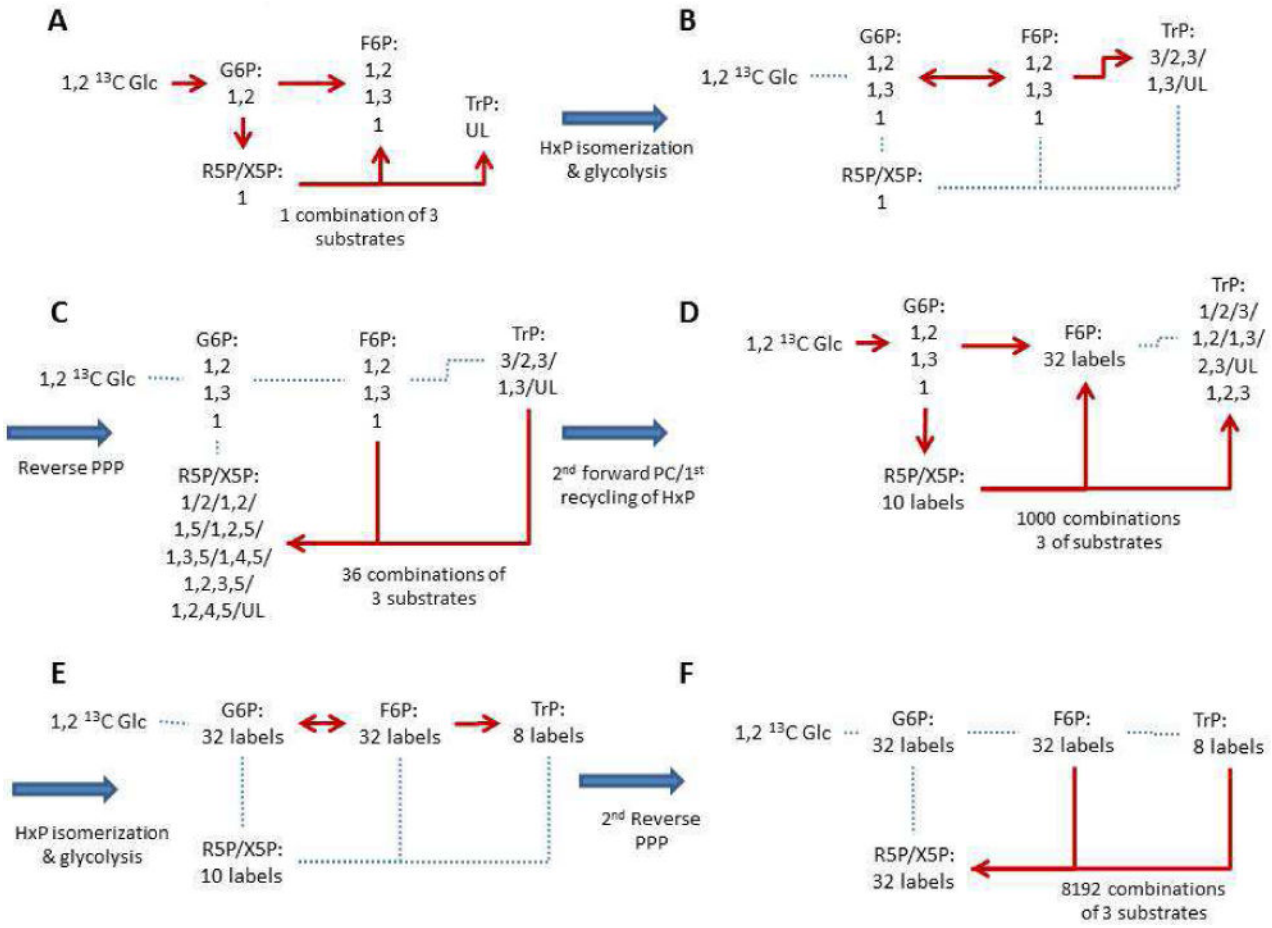

Figure 3.

Reaction sequence for computations of ^{13}C distribution in hexose phosphates, pentose phosphates, and triose phosphates. (A) The first forward reaction of the pentose cycle occurs. The fractional contents of R5P/X5P, F6P, and TrP are calculated from metabolism of exogenous [1,2-$^{13}C_2$]glucose through the oxidative and forward non-oxidative PPP. Numbers below each metabolite indicate ^{13}C position within the metabolite. A metabolite not enriched in ^{13}C is indicated as unlabeled (UL). (B) Isomerization of F6P to G6P and glycolytic production of TrP occurs. Triose phosphate composition is updated as HxP from exogenous glucose and the non-oxidative PPP are metabolized through glycolysis and combine with TrP from the pentose cycle. (C) The first reverse non-oxidative PPP occurs. The content of R5P/X5P is updated as ten new labels enter the pentose phosphate pool from reverse non-oxidative PPP flux and combine with the existing label from the oxidative PPP. The content of each new label is calculated from the 36 possible combinations of two F6P and one TrP. (D) The second forward pentose cycle occurs. Updated calculations to the fractional contents of R5P/X5P, F6P, and TrP pools are implemented as HxP recycling begins. The R5P/X5P pool is updated as the oxidative PPP produces additional labels from the recycled HxP. This is followed by updates to F6P and TrP composition as 1000 possible combinations of pentose phosphates occur in the forward non-oxidative PPP. (E, F) Updates to the TrP (E) and pentose phosphate (F) pools are calculated as glycolysis and reverse flux

through the non-oxidative PPP occur to alter their compositions. This sequential series of calculations is repeated for six rounds of forward recycling/reverse PPP flux to obtain the final composition of TrP, and thus pyruvate, derived from glycolysis.

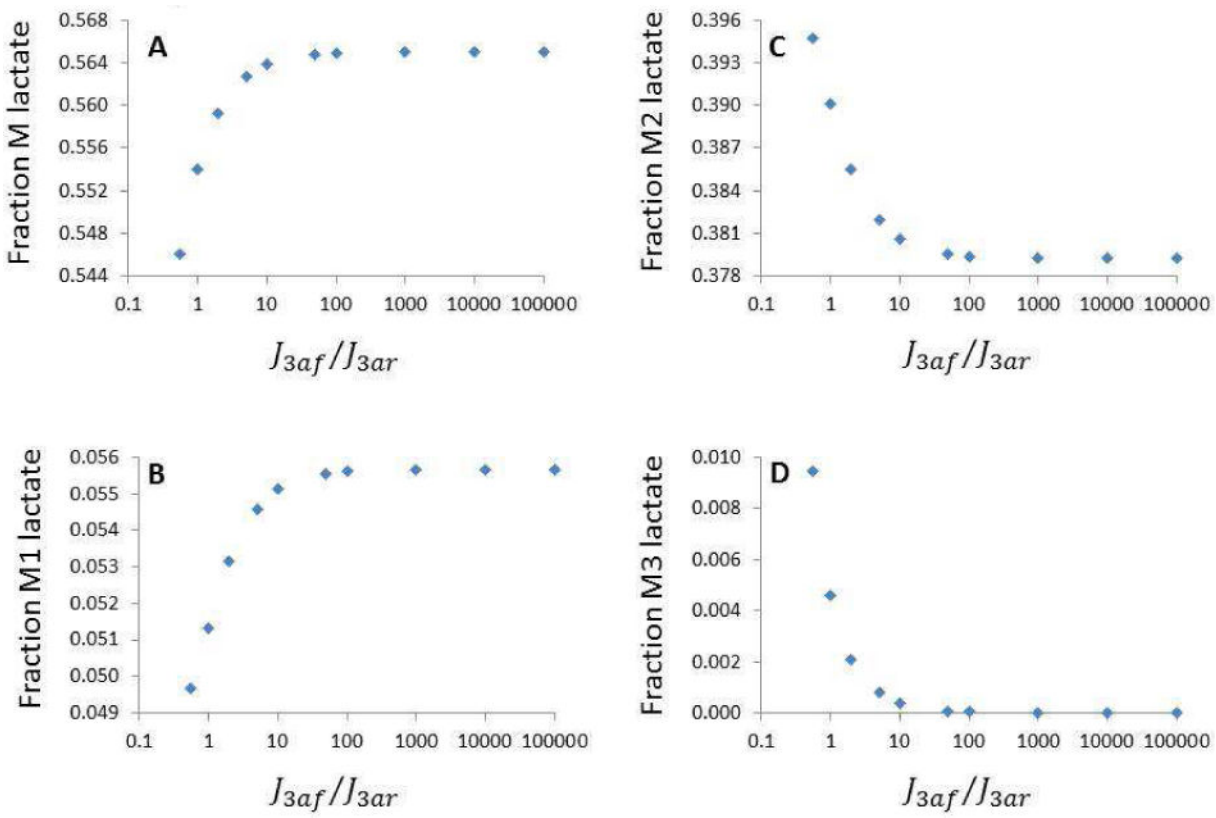

Figure 4.

Effect of reverse non-oxidative PPP flux on ^{13}C distribution in lactate. The ratio of forward (J_{3af}) to reverse (J_{3ar}) non-oxidative PPP flux was incorporated as a model-optimized parameter affecting the fraction of unlabeled (M), single- (M1), double- (M2), and triple- (M3) ^{13}C labeled lactate. The remaining three optimized parameters were kept constant: $J_{3af}/(J_0 + J_{3af}) = 0.25$, $J_7/(J_{2b} + J_7) = 0$, $J_5 = 94$. The fluxes for this analysis were: $J_0 = 291$, $J_4 = 288$, $J_{RR} = 564$ pmol glucose, lactate, or atomic oxygen used or produced per minute per 10^6 cells, respectively. Table 1 shows the corresponding changes in labeling the hexose and pentose phosphate pools for the same parameters and flux inputs used here.

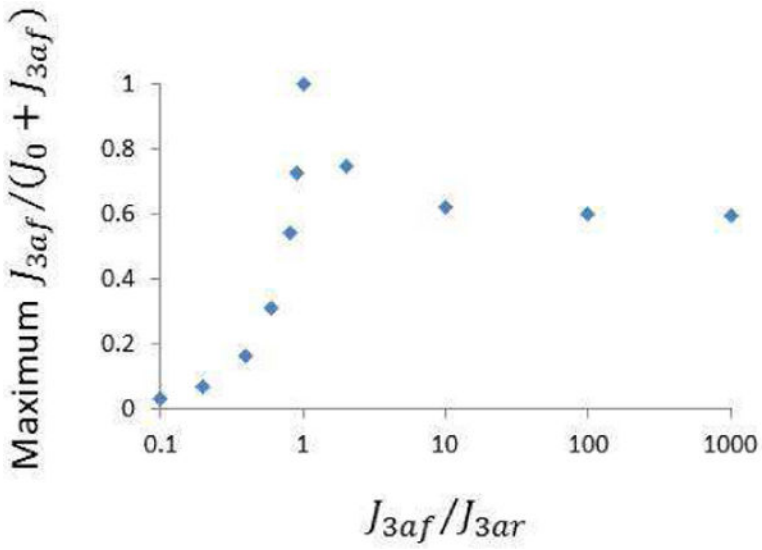

Figure 5.

Maximum contribution of the forward non-oxidative PPP to labeling the HxP pool depends on the rate of reverse flux through the non-oxidative PPP. Lactate labeling is affected by the relative contributions of the forward non-oxidative PPP (J_{3af}) and glucose uptake/phosphorylation (J_0) to total HxP produced ($J_{3af}/(J_0 + J_{3af})$ and $1 - [J_{3af}/(J_0 + J_{3af})]$, respectively), as well as by the ratio of forward to reverse non-oxidative PPP flux (J_{3af}/J_{3ar}). The relationship between the two ratios was assessed by determining the maximum possible value that could be assigned to $J_{3af}/(J_0 + J_{3af})$ for variations in J_{3af}/J_{3ar}. The maximum occurred when $J_9 < 0$ for $J_{3af}/J_{3ar} > 1$ or $J_1 < 0$ for $J_{3af}/J_{3ar} < 1$. When implemented to find solutions for these variables, the model does not exceed these maximums because of explicit constraints that all fluxes must be non-negative. This relationship was assessed assuming the following conditions: $J_0 = 291\ pmol\frac{glc}{min}$, $J_4 = 288\ pmol\frac{lac}{min}$, $J_{RR} = 567\ pmol\frac{o}{min}$, $J_5 = 97\ pmol\frac{pyr}{min}$, and $J_7/(J_{2b}+J_7) = 0.05$.

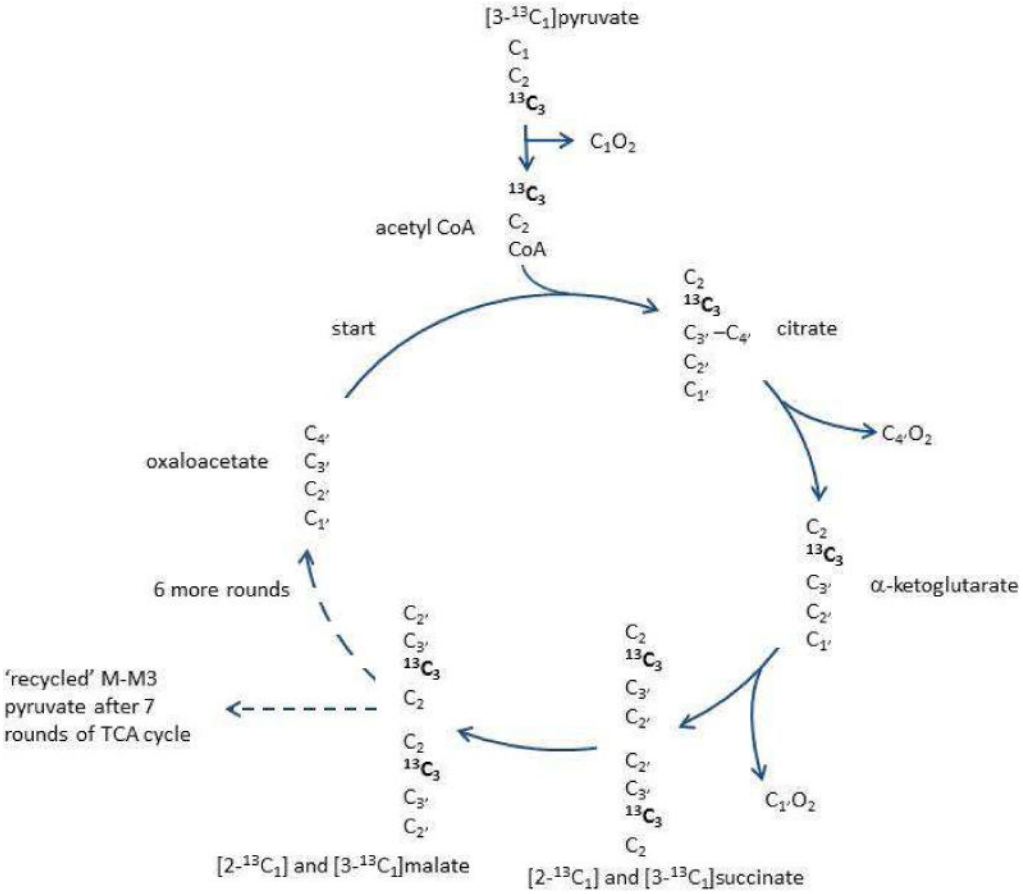

Figure 6.

Carbon reshuffling in the tricarboxylic acid (TCA) cycle. The carbon atom transitions are depicted for select metabolites in the TCA cycle as unlabeled oxaloacetate reacts with acetyl-CoA derived from [3-$^{13}C_1$]pyruvate in this example for the first of seven rounds used to evaluate malate labeling. Succinate dehydrogenase does not distinguish between carboxylic acid carbons 1 and 4 in succinate since it is symmetrical, so there is a 50% chance that ^{13}C in malate will reside at position 2 or 3. This aspect of carbon reshuffling in the TCA cycle was overlooked in the original model. The labeled malate from the first round is subjected to six more rounds of the cycle, each time reacting with an acetyl-CoA label derived from the pyruvate pool. From this, fractional pyruvate labeling generated by malic enzyme is determined.

Neurochem Int. Author manuscript; available in PMC 2018 October 01.

Table 1

Effect of reverse non-oxidative PPP flux on hexose and pentose phosphate pools with [1,2$^{13}C_2$]glucose.

	Fractional ^{13}C in Hexose Phosphates						
J_{3af}/J_{3ar}	**M**	**M1**	**M2**	**M3**	**M4**	**M5**	**M6**
100000	0.0036	0.1275	0.8688	<0.0001	<0.0001	<0.0001	<0.0001
10000	0.0036	0.1275	0.8688	<0.0001	<0.0001	<0.0001	<0.0001
1000	0.0036	0.1275	0.8688	<0.0001	<0.0001	<0.0001	<0.0001
100	0.0036	0.1274	0.8688	<0.0001	<0.0001	<0.0001	<0.0001
50	0.0037	0.1272	0.8689	0.0002	<0.0001	<0.0001	<0.0001
10	0.0039	0.1258	0.8691	0.0008	0.0003	0.0002	<0.0001
5	0.0041	0.1242	0.8692	0.0017	0.0005	0.0003	<0.0001
2	0.0047	0.1197	0.8692	0.0043	0.0012	0.0009	<0.0001
1	0.0054	0.1137	0.8676	0.0091	0.0022	0.0020	<0.0001
0.55	0.0059	0.1074	0.8613	0.0181	0.0032	0.0042	<0.0001
	Fractional ^{13}C in Pentose Phosphates						
J_{3af}/J_{3ar}	M	M1	M2	M3	M4	M5	
100000	0.1246	0.8724	0.0029	<0.0001	<0.0001	<0.0001	
10000	0.1246	0.8724	0.0029	<0.0001	<0.0001	<0.0001	
1000	0.1247	0.8720	0.0032	<0.0001	<0.0001	<0.0001	
100	0.1254	0.8680	0.0056	0.0003	0.0006	<0.0001	
50	0.1261	0.8636	0.0083	0.0006	0.0013	<0.0001	
10	0.1320	0.8288	0.0296	0.0032	0.0064	<0.0001	
5	0.1394	0.7859	0.0557	0.0062	0.0127	<0.0001	
2	0.1617	0.6612	0.1309	0.0147	0.0313	0.0002	
1	0.1988	0.4662	2465	0.0268	0.0609	0.0007	
0.55	0.2574	0.1797	0.4127	0.0420	0.1056	0.0025	

The measured fluxes used for the calculations were from (Gebril et al 2016): J_0 = 291, J_4 = 288, J_{RR} = 564 pmol glucose, lactate, or atomic oxygen used or produced per minute per 10^6 cells, respectively. The model inputs kept constant were: $J_{3af}/(J_0 + J_{3af})$ = 0.25, $J_7/(J_{2b} + J_7)$ = 0, J_5 = 94. The fraction of hexose (G6P, F6P) or pentose (R5P, X5P) phosphates having none (M), one (M1), or more (M2-M6) ^{13}C atoms was calculated from Eq. 4 and 5, respectively.

Neurochem Int. Author manuscript; available in PMC 2018 October 01.

Table 2

Symmetrical vs. non-symmetrical succinate metabolism in the TCA cycle.

Updated TCA cycle: symmetrical						**Original TCA cycle: non-symmetrical**					
	Fractional ^{13}C in malate						**Fractional ^{13}C in malate**				
$\frac{J_7}{J_{2b}+J_7}$	**M**	**M1**	**M2**	**M3**	**M4**	$\frac{J_7}{J_{2b}+J_7}$	**M**	**M1**	**M2**	**M3**	**M4**
0.01	0.1864	0.3115	0.2633	0.1797	0.0590	0.01	0.1821	0.3117	0.2643	0.1810	0.0610
0.02	0.1862	0.3118	0.2641	0.1794	0.0586	0.02	0.1818	0.3120	0.2651	0.1807	0.0605
0.05	0.1855	0.3128	0.2664	0.1783	0.0571	0.05	0.1810	0.3128	0.2675	0.1797	0.0590
0.10	0.1844	0.3146	0.2702	0.1762	0.0546	0.10	0.1799	0.3144	0.2714	0.1779	0.0565
0.15	0.1836	0.3166	0.2739	0.1739	0.0520	0.15	0.1789	0.3162	0.2751	0.1758	0.0539
0.20	0.1830	0.3189	0.2774	0.1713	0.0494	0.20	0.1782	0.3183	0.2788	0.1735	0.0513
	Fractional ^{13}C in pyruvate from ME						Fractional ^{13}C in pyruvate from ME				
$\frac{J_7}{J_{2b}+J_7}$	M	M1	M2	M3		$\frac{J_7}{J_{2b}+J_7}$	M	M1	M2	M3	
0.01	0.2561	0.3614	0.2741	0.1084		0.01	0.3203	0.3052	0.2333	0.1413	
0.02	0.2560	0.3620	0.2741	0.1078		0.02	0.3195	0.3062	0.2339	0.1403	
0.05	0.2558	0.3641	0.2742	0.1058		0.05	0.3172	0.3095	0.2359	0.1374	
0.10	0.2556	0.3677	0.2742	0.1025		0.10	0.3136	0.3149	0.2390	0.1324	
0.15	0.2557	0.3714	0.2739	0.0991		0.15	0.3102	0.3206	0.2418	0.1274	
0.20	0.2560	0.3752	0.2733	0.0955		0.20	0.3071	0.3264	0.2443	0.1222	
	Fractional ^{13}C in exported lactate						Fractional ^{13}C in exported lactate				
$\frac{J_7}{J_{2b}+J_7}$	M	M1	M2	M3		$\frac{J_7}{J_{2b}+J_7}$	M	M1	M2	M3	
0.01	0.5613	0.0581	0.3791	0.0015		0.01	0.5619	0.0576	0.3787	0.0018	
0.02	0.5587	0.0611	0.3776	0.0025		0.02	0.5600	0.0600	0.3768	0.0032	
0.05	0.5510	0.0703	0.3731	0.0057		0.05	0.5541	0.0675	0.3711	0.0072	
0.10	0.5382	0.0858	0.3655	0.0106		0.10	0.5440	0.0805	0.3620	0.0136	

Updated TCA cycle: symmetrical						Original TCA cycle: non-symmetrical					
	Fractional ^{13}C in malate						Fractional ^{13}C in malate				
$\frac{J_7}{J_{2b}+J_7}$	M	M1	M2	M3	M4	$\frac{J_7}{J_{2b}+J_7}$	M	M1	M2	M3	M4
0.15	0.5253	0.1016	0.3579	0.0152		0.15	0.5335	0.0940	0.3531	0.0194	
0.20	0.5126	0.1179	0.3502	0.0194		0.20	0.5228	0.1081	0.3444	0.0247	

The measured fluxes used for the calculations were from (Gebril et al 2016): J_0 = 291, J_4 = 288, J_{RR} = 564 pmol glucose, lactate, or atomic oxygen used or produced per minute per 10^6 cells, respectively. The model inputs kept constant were: J_{3af}/J_{3ar} = 10, $J_{3af}/(J_0 + J_{3af})$ = 0.25. The updated TCA cycle accounts for ^{13}C randomization in malate as a result of succinate symmetry as it is metabolized in the TCA cycles, whereas the original model assumed carbons 1 and 2 of succinate remained exclusively at these positions in malate. The fraction of malate having none (M), one (M1), or more (M2-M4) ^{13}C atoms was calculated from Eq. 9. Pyruvate labeling from malic enzyme (ME) was calculated as the sum of all malate labels that, when decarboxylated at carbon 4, yield each specific pyruvate label. Labeling in exported lactate accounts for the contribution of ME, glycolysis and pentose cycle-derived triose phosphate to the pyruvate pool.

Table 3

Re-analysis of ^{13}C distribution in lactate from cerebellar granule neurons by LC-TQMS.

	Area				Fractional ^{13}C distribution			
[^{12}C Lac] (μM)	**M**	**M1**	**M2**	**M3**	**M**	**M1**	**M2**	**M3**
100	10732	221	39	0	0.9764	0.0201	0.0035	0.0000
200	21810	658	71	0	0.9677	0.0292	0.0031	0.0000
400	44146	1300	200	0	0.9671	0.0285	0.0044	0.0000
600	62110	2099	264	4	0.9633	0.0326	0.0041	0.0001
800	83522	2897	352	2	0.9625	0.0334	0.0041	0.0000
[$^{13}C_1$ Lac] (μM)	M	M1	M2	M3	M	M1	M2	M3
100	218	11485	292	13	0.0182	0.9564	0.0243	0.0011
200	394	23596	484	65	0.0160	0.9616	0.0197	0.0027
400	0	45987	1154	144	0.0000	0.9726	0.0244	0.0030
600	671	74063	1596	271	0.0088	0.9669	0.0208	0.0035
800	875	96330	2310	310	0.0088	0.9650	0.0231	0.0031
[^{12}C:$^{13}C_1$ Lac] @ 7.6:1	M	M1	M2	M3	M	M1	M2	M3
100	10032	1339	82	0	0.8759	0.1169	0.0072	0.0000
200	19940	2989	131	5	0.8645	0.1296	0.0057	0.0002
400	40238	6144	246	13	0.8627	0.1317	0.0053	0.0003
600	57760	8990	381	29	0.8600	0.1339	0.0057	0.0004
800	75337	11686	472	13	0.8609	0.1335	0.0054	0.0001
	[lactate] (mM)				Fractional ^{13}C distribution			
samples	M	M1	M2	M3	M	M1	M2	M3
^{13}C glc + cells	202±37	10±2	207±39	5.0±0.8	0.4751±0.0021	0.0249±0.0007	0.4881±0.0021	0.0119±0.0004
^{12}C glc + cells	417±66	14±2	3.7±0.4	0.9±0.0	0.9556±0.0016	0.0335±0.0010	0.0088±0.0005	0.0022±0.0003

Lactate produced by cerebellar granule neurons (7×10^6 cells cultured in 2-well Lab-Tek chambers; n=5) after 5 hr incubation with 9.6mM ^{12}C or [1,2-$^{13}C_2$] glucose were extracted with methanol and derivatized with 3-nitrophenylhydrazine. Ions 224, 225, 226, and 227 Da corresponding to derivatized lactate M, M1, M2, and M3, respectively, were separated and quantitated by liquid chromatography

triple quadrupole mass spectrometry. The areas have been background subtracted using cell-free media without exogenous lactate. Lactate M and M2 concentrations were calculated from 100–800 μM M1 standards (corrected for M1 purity of 0.9625). Lactate M1 and M3 concentrations were calculated from 12–98 μM M1 standards derived from the M:M1 mixture.

Table 4

Cerebellar granule neuron fluxes estimated from the updated model.

	Optimized Flux Ratio		
	J_{3af}/J_{3ar}	$J_{3af}/(J_0+J_{3ar})$	$J_7/(2J_{2a}+J_{3bf}+J_7)$
Model Result	**nd**	**<0.0001±0.0000 (<0.0001–0.0023)**	**0.0782±0.0000 (0.0691–0.0803)**

	Fractional ^{13}C distribution in lactate			
	M	**M1**	**M2**	**M3**
Model result	0.4755±0.0000 (0.4749–0.4784)	0.0249±0.0000 (0.0220–0.0256)	0.4857±0.0000 (0.4850–0.4872)	0.0140±0.0000 (0.0124–0.0143)
Measured	0.4751±0.0021	0.0249±0.0007	0.4881±0.0021	0.0119±0.0004
error	0.0004 (0.0002–0.0030)	<0.0001 (<0.0001–0.0013)	0.0024 (0.0006–0.0040)	0.0021 (0.0011–0.0034)

Reaction block	Flux, set 1 (J_{3af}/J_{3ar} = *max*) (pmol/min × 10^6 cells)	Flux, set 2 (J_{3af}/J_{3ar} = *min*) (pmol/min × 10^6 cells)
Glucose uptake (J_0)	291±23	291±23
Oxidative PPP (J_1)	112±24 (111–113)	0±0
Glycolysis, upper (J_{2a})	178±23 (178–180)	201±21
Glycolysis, lower (J_{2b})	357±45 (356–361)	357±45
Non-oxidative PPP, for. (J_{3f})	0±0 (0–1.1)	0±0
Non-oxidative PPP, rev. (J_{3r})	0±0 (0–1.1)	135±30
Lactate production (J_4)	288±46	288±46
Pyruvate oxidation (J_5)	99±5 (98–99)	99±5
NADH oxidation (J_6)	67±4 (67–72)	67±4
Cyto. malic enzyme (J_7)	30±4 (26–31)	30±4
NADPH oxidation (J_8)	255±47 (247–257)	30±4
Nucleotide synthesis (J_9)	112±24 (110–113)	135±30
Mito. respiration (J_{RR})	564±29	564±29

Measured fluxes (J_0,J_4,J_{RR}; mean±standard error of the mean, n=6) from (Gebril et al., 2016) and re-measured fractional ^{13}C distribution in lactate (M-M3; mean±standard error of the mean, n=5) were used to solve for the remaining fluxes (expressed as pmol substrate consumed, except for J_{3r} which is pmol product formed) by optimizing the three flux ratios and J_5. The model results reflect minimization of the total error between the predicted and measured values. J_{3af}/J_{3ar} could not be determined (nd) from the data given J_{3af} was negligible (J_{3af} = 0.0029 ± 0.0002 pmol F6P/min × 10^6 cells from the constraint that $J_{3af}/(J_0 + J_{3af}) \geq 0.00001$). Set 1 fluxes assumed the maximum possible ratio (i.e., the same negligible reverse as forward non-oxidative PPP flux so that J_{3af}/J_{3ar} = 1) while set 2 fluxes assumed a minimum possible ratio (which averaged 4.29±1.02 × 10^{-5}; maximal J_{3ar} was reached when oxidative PPP flux was < 0.01 pmol G6P/min × 10^6 cells). The maximum and minimum ratios

therefore provide a range of uncertainties for the five fluxes (J_1,J_{2a},J_{3r},J_8,J_9) dependent on J_{3af}/J_{3ar}. Numbers in parentheses reflect the highest and lowest means from 100 Monte Carlo simulated data sets for $J_{3ar} = J_{3af}$. The simulations were not performed for $J_{3af}/J_{3ar} = min$ as the variation was expected to be similar given virtually no contribution of J_{3af} to labeling the hexose phosphate pool.